Band-structure effects in photoelectron-emission spectra from metal surfaces

C. A. Rios Rubiano and M. S. Gravielle
Instituto de Astronomía y Física del Espacio (CONICET-UBA), Casilla de correo 67, sucursal 28, 1428 Buenos Aires, Argentina

D. M. Mitnik
Instituto de Astronomía y Física del Espacio (CONICET-UBA), Casilla de correo 67, sucursal 28, 1428 Buenos Aires, Argentina and Departamento de Física, FCEyN, Universidad de Buenos Aires, Buenos Aires, Argentina

V. M. Silkin
Donostia International Physics Center, 20018 San Sebastián, Spain, Departameto de Física de Materiales, Facultad de Ciencias Químicas, Universidad del País Vasco, Apartado 1072, 20080 San Sebastián, Spain, and IKERBASQUE, Basque Foundation for Science, 48011 Bilbao, Spain
(Received 10 February 2012; published 24 April 2012)

Photoelectron emission from the valence band of a metal surface due to the grazing incidence of ultrashort laser pulses is studied in the framework of a distorted-wave formulation. We propose a model, named the band-structure-based–Volkov (BSB-V) approximation, which takes into account the contribution of the band structure of the solid. The BSB-V approach is applied to calculate differential electron-emission probabilities for Al(111) and Be(0001) surfaces. A noticeable influence of the electronic band structure was observed in the case of beryllium, while for aluminum such effects were found to play a minor role.

DOI: 10.1103/PhysRevA.85.043422 PACS number(s): 32.80.Wr, 79.60.−i, 78.66.Bz

I. INTRODUCTION

The fast development of new technologies has made it possible to generate shorter and more intense laser pulses, enabling the investigation of electrons in condensed matter in their natural temporal domain [1]. Experimentally, ultrashort pump-probe spectroscopy is one of the tools used to study the dynamic behavior of electrons in the bulk and the near surface of solids [1–6]. The application of such a method requires the primary determination of electron-emission spectra produced by incidence of laser pulses with high frequencies and time durations in the subfemtosecond range [1,4,7–10]. This article deals precisely with double-differential (energy- and angle-resolved) distributions of electrons emitted from the valence band of metal surfaces by interaction with few-cycle electromagnetic pulses with high carrier frequencies. Our aim is to investigate the role played by band structure effects, focusing special attention on the contribution coming from the partly occupied surface electronic states (SESs) which are present on many metal surfaces [11–13].

To describe photoinduced electron emission from a metal surface we introduce a time-dependent distorted-wave approach, named band-structured-based–Volkov (BSB-V) approximation. This method includes a realistic description of the electron-surface interaction given by the band-structure-based (BSB) model [14], while the action of the laser field on the emitted electron is represented by means of the Volkov phase [15]. The BSB model is based on the one-dimensional pseudopotential proposed by Chulkov *et al*. [14,16], which incorporates information about the band structure of the solid, reproducing the width and position of the projected bulk energy gap and the energies of the surface and first image-potential states [17–21]. This kind of potential has been successfully applied in different branches of investigation [21–33]. On the other hand, the use of the well-known Volkov phase within one-active-electron theories, like the one proposed here, has shown to provide reasonable predictions for different laser-induced electron-emission processes from metal surfaces [34–37]. The BSB-V approximation represents a reliable alternative approach to the numerical solution of the time-dependent Schrödinger equation (TDSE) [38], with the advantage that it allows us to extract easily information about the different mechanisms.

In this article, the BSB-V method is applied to evaluate electron-emission spectra from Al(111) and Be(0001). Both surfaces present partly occupied SESs with energies in the vicinity of the Fermi level. In particular, the Be(0001) surface shows a strong corrugation of the potential inside the material, which affects the electronic density, giving rise to a SES with an exceptionally high electron density localization near the surface atomic layer [39]. This fact will be used to study the relative importance of the contribution of SESs in photoinduced electron-emission spectra. Indeed, it has recently been found that this kind of partly occupied SES can dramatically modify the dielectric properties of metal surfaces [40–42] and originate noticeable structures in electron distributions produced by projectile impact [43]. For monochromatic electromagnetic radiation, photoemission from the SESs of Al(111) and Be(0001) surfaces was studied within a one-step model in Refs. [44,45].

To corroborate the validity of the BSB-V approximation, results are compared with the numerical solution of the TDSE derived under the same conditions, that is, by using the BSB model to represent the surface interaction. In addition, in order to estimate the relevance of the proper description of the surface potential, electron spectra derived with a simpler model, the impulsive jellium-Volkov (IJV) approximation, are also presented [34]. The IJV approach involves a plain representation of the surface interaction given by the jellium model.

The work is organized as follows. In Sec. II we derive the BSB-V approximation from the time-dependent distorted-wave formalism. In Sec. III, results are presented and discussed, and the conclusions are summarized in Sec. IV. Atomic units are used unless otherwise stated.

II. THEORY

Let us consider a laser pulse, characterized by a time-dependent electric field $\mathbf{F}(t)$, impinging grazingly on a metal surface S. As a consequence of this interaction, an electron e of the valence band of the solid, initially in the state Φ_i, is ejected above the vacuum level, ending in the final state Φ_f. In the presence of the external electric field, the temporal evolution of the electronic state is governed by the Hamiltonian

$$H(t) = H_0 + \mathbf{r}\cdot\mathbf{F}(t) + V_{\rm ind}(\mathbf{r},t), \tag{1}$$

where $H_0 = -\nabla^2/2 + V_S(\mathbf{r})$ is the unperturbed Hamiltonian, with $\mathbf{r}$ being the position vector of the active electron e and V_S being the electron-surface interaction. The second term of Eq. (1) represents the interaction potential with the laser, expressed in the length gauge, while $V_{\rm ind}$ denotes the surface-induced potential that is produced by electronic density fluctuations originated by the external laser field. The frame of reference is placed at the surface border, which is shifted with respect to the position of the topmost atomic layer by half of the interplanar distance. The $\hat{z}$ axis is oriented perpendicular to the surface, pointing toward the vacuum region.

In this work we employ the BSB model to represent the electron interaction with the metal surface. Within this model, translational invariance in the plane parallel to the surface is assumed, with V_S being defined as a one-dimensional potential depending on the component of $\mathbf{r}$ perpendicular to the surface z. Then, the eigenfunctions of H_0 are expressed as

$$\Phi_{\mathbf{k}_s,n}(\mathbf{r},t) = \frac{1}{2\pi}\exp(i\mathbf{k}_s\cdot\mathbf{r}_s)\,\phi_n(z)e^{-iEt}, \tag{2}$$

where $\mathbf{k}_s$ ($\mathbf{r_s}$) is the component of the electron momentum (position vector) parallel to the surface plane and $E = k_s^2/2 + \varepsilon_n$ is the electron energy. The one-dimensional function $\phi_n(z)$ and its corresponding eigenenergies ε_n are obtained by solving the one-dimensional Schrödinger equation associated with the realistic pseudopotential of Ref. [14], which takes into account the influence of the band structure of the material. Using slab geometry, the functions ϕ_n are expressed as

$$\phi_n(z) = \frac{1}{\sqrt{L}}\sum_{j=-N}^{N} a_n(j)\exp\left[i\frac{2\pi j}{L}(z+d_s)\right] \tag{3}$$

for $|z+d_s| < L/2$ and 0 elsewhere, where L is a normalization length, $2N+1$ is the number of basis functions, and d_s is the distance between the center of the slab and the surface edge. In Eq. (3) the coefficients $a_n(j)$ are numerically evaluated by employing a supercell technique.

Taking into account the grazing incidence condition together with the translational invariance of V_S in the direction parallel to the surface, we consider a linear polarized laser pulse with $\mathbf{F}(t)$ oriented perpendicular to the surface plane, i.e., along the $\hat{z}$ axis. The temporal profile of the pulse is defined as

$$F(t) = F_0\sin(\omega t+\varphi)\sin^2(\pi t/\tau) \tag{4}$$

for $0 < t < \tau$ and 0 elsewhere, where F_0 is the maximum field strength, ω is the carrier frequency, φ represents the carrier envelope phase, and τ determines the duration of the pulse. The phase φ is chosen as $\varphi = -\omega\tau/2 + \pi/2$ to obtain a symmetric pulse that verifies $F(t) = F(\tau - t)$. For pulses containing an integer number of cycles inside the envelope, the duration of the pulse is $\tau = n\,2\pi/\omega$, with n being the number of cycles.

A. BSB-V transition amplitude

Making use of the time-dependent distorted-wave formalism, the BSB-V amplitude for the electronic transition $\Phi_i \to \Phi_f$ can be expressed as

$$\mathcal{A}_{if} = -i\int_{-\infty}^{+\infty} dt\,\langle\chi_f|\mathcal{V}(t)|\Phi_i\rangle, \tag{5}$$

where $\Phi_i \equiv \Phi_{\mathbf{k}_{is},n_i}(\mathbf{r},t)$ is the initial unperturbed state, given by Eq. (2), $\mathcal{V}(t) = \mathbf{r}\cdot\mathbf{F}(t) + V_{\rm ind}(\mathbf{r},t)$ is the corresponding perturbative potential, and χ_f is the final distorted-wave function derived within the BSB-V model. The function χ_f is obtained from the momentum distribution of the final state $\Phi_f \equiv \Phi_{\mathbf{k}_{fs},n_f}(\mathbf{r},t)$ by including the action of the laser field through the phase of the Volkov function. It reads [46]

$$\begin{aligned}\chi_f(\mathbf{r},t) &= (2\pi)^{-3/2}\int d\mathbf{q}\,e^{i\mathbf{q}\cdot\mathbf{r}}\,\widetilde{\Phi}_{\mathbf{k}_{fs},n_f}(\mathbf{q},t)\exp[iD_L^-(\mathbf{q},\mathbf{r},t)]\\ &= \Phi_{\mathbf{k}_{fs},n_f}(\mathbf{r}-\alpha^-(t),t)\exp[iD_L^-(\mathbf{0},\mathbf{r},t)],\end{aligned} \tag{6}$$

where the tilde denotes the Fourier transformation in momentum space. The Volkov phase originated by the laser electric field is expressed as [15]

$$D_L^-(\mathbf{q},\mathbf{r},t) = \mathbf{A}^-(t)\cdot\mathbf{r} - \beta^-(t) - \mathbf{q}\cdot\alpha^-(t), \tag{7}$$

where

$$\begin{aligned}\mathbf{A}^-(t) &= -\int_{+\infty}^{t} dt'\mathbf{F}(t'),\\ \beta^-(t) &= 2^{-1}\int_{+\infty}^{t} dt'[\mathbf{A}^-(t')]^2,\\ \alpha^-(t) &= \int_{+\infty}^{t} dt'\mathbf{A}^-(t')\end{aligned} \tag{8}$$

are related to the vector potential, the ponderomotive energy, and the quiver amplitude, respectively, and the minus sign accounts for the asymptotic conditions.

For frequencies higher than the surface-plasmon frequency ω_s, the induced surface potential associated with the response of the surface to the external field is much smaller than the laser interaction. Consequently, its effect on the perturbative potential $\mathcal{V}(t)$ can be neglected [47]. We also neglect the time-dependent induced potential originated by the emitted electron [48], whose contribution is reduced by transient dynamic effects [49,50]. Under these assumptions the transition amplitude reduces to

$$\mathcal{A}_{if} = \delta(\mathbf{k}_{fs} - \mathbf{k}_{is})\,a_{if}, \tag{9}$$

where the Dirac delta function imposes the momentum conservation in the direction parallel to the surface and

$$a_{if} = -i \int_0^\tau dt\, \exp[i\Delta\varepsilon t + \beta^-(t)] F(t)\, R_{if}(t) \qquad (10)$$

is the one-dimensional transition amplitude, with $\Delta\varepsilon = \varepsilon_{n_f} - \varepsilon_{n_i}$ being the energy gained by the electron during the process. The function $R_{if}(t)$ represents the one-dimensional form factor given by

$$R_{if}(t) = \int_{-\infty}^{+\infty} dz\, z\, \phi^*_{n_f}(z - \alpha^-(t)) \phi_{n_i}(z) g_f(z) \exp[-iA^-(t)z], \qquad (11)$$

where the function $g_f(z) = e^{z\Theta(-z)/(2\lambda_f)}$ has been introduced to incorporate the stopping of the ionized electron inside the material [36], with $\lambda_f = \lambda\left(E_f\right)$ being the energy-dependent electron mean free path, $E_f = k_{fs}^2/2 + \varepsilon_{n_f}$ being the final electron energy, and Θ being the unitary Heaviside function. By replacing the one-dimensional wave functions of Eq. (3) in Eq. (11), $R_{if}(t)$ displays a closed form in terms of the field functions $A^-(t)$ and $\alpha^-(t)$.

B. BSB-V differential probability

The double-differential probability of electron emission from the surface can be expressed in terms of the transition amplitude given by Eq. (9) as

$$\frac{d^2P}{dE_f d\Omega_f} = k_f \sum_i 2|\mathcal{A}_{if}|^2, \qquad (12)$$

where $\Omega_f = (\theta_f, \varphi_f)$ is the solid angle determined by the final electron momentum $\mathbf{k}_f$, with θ_f and φ_f being the polar and azimuthal angles, respectively, and $k_f = |\mathbf{k}_f|$. In Eq. (12) the sum indicates the addition over all possible initial states, with the factor 2 taking into account the spin states.

Since the final electronic state $\Phi_{\mathbf{k}_{fs}, n_f}$ displays a well-defined momentum only in the direction parallel to the surface, the final momentum vector $\mathbf{k}_f = (\mathbf{k}_{fs}, k_{fz})$ is obtained by defining an *effective* electron momentum perpendicular to the surface as $k_{fz} = \sqrt{2\varepsilon_{n_f}}$. Note that as a result of the translational invariance parallel to the surface of the problem, the double-differential probability given by Eq. (12) does not vary with the azimuthal angle φ_f, depending only on the elevation angle $\theta_f = \sin^{-1}(k_{fz}/k_f)$ that is measured with respect to the surface plane.

After some steps of algebra that involve the standard treatment for the square of the δ function [51], the differential probability reads

$$\frac{d^2P}{dE_f d\Omega_f} = 2k_f\, \rho(k_{fz}) \sum_{n_i} |a_{if}|^2 \Theta(-\varepsilon_{n_i} - E_W) \Theta(\widetilde{k}_{n_i} - k_{fs}), \qquad (13)$$

where $\rho(k_{fz})$ is the density of final states ϕ_{n_f} with perpendicular momentum k_{fz}. In Eq. (13), the first unitary Heaviside function $\Theta(-\varepsilon_{n_i} - E_W)$ restricts the initial states to those contained within the Fermi surface, with E_W being the work function, while the second one, $\Theta(\widetilde{k}_{n_i} - k_{fs})$, is originated by the momentum conservation parallel to the surface, with $\widetilde{k}_{n_i} = \sqrt{-2(\varepsilon_{n_i} + E_W)}$.

III. RESULTS

In this article the BSB-V approximation is employed to evaluate photoelectron-emission spectra from Al(111) and Be(0001) surfaces. Taking into account that the carrier frequency represents a key parameter for photoinduced electron-emission processes, electron distributions are analyzed in terms of ω, considering ω values larger than the surface-plasmon frequency. In all the cases we kept the number of cycles of the laser electric field inside the envelope as a constant. In particular, we chose six-cycle laser pulses (with $n = 6$) [8,36]. The field strength was fixed at $F_0 = 0.001$ a.u., which corresponds to the intensity $I \simeq 3.5 \times 10^{10}$ W/cm^2, which belongs to the perturbative regime, far from the saturation region and the damage threshold [3,5,52].

BSB-V energy- and angle-resolved electron distributions were evaluated from Eq. (13). In the calculation of a_{if}, the numerical integration on time involved in Eq. (10) was done with a relative error lower than 0.1%. In addition, since the one-dimensional wave functions given by Eq. (3) do not allow us to distinguish electrons emitted inside the solid from those ejected toward the vacuum region, as a first estimation we averaged the contributions from the two different wave functions $\phi_{n_f}(z)$ associated with the same positive energy ε_{n_f} by considering that ionized electrons emitted to the vacuum region represent approximately 50% of the total ionized electrons from the conduction band [53].

A. Electron emission from Al(111)

Our first goal is to study the performance of the BSB-V approximation for aluminum, which is a typical metal surface that can be used as a benchmark for the theory. The Al(111) surface is characterized by a Fermi energy $E_F = 0.414$ a.u., a work function $E_W = 0.156$ a.u., an interplanar distance of 4.388 a.u., and a surface-plasmon frequency $\omega_s = 0.4$ a.u. For Al, the BSB wave functions given by Eq. (3) were obtained by using a basis of plane waves with $N = 170$, a unit cell of width $L = 394.92$ a.u., and a distance between the crystal border and the center of the slab $d_s = 155.77$ a.u. The energy-dependent electron mean free path in the aluminum bulk was extracted from Ref. [54].

In Fig. 1 we show BSB-V differential electron-emission probabilities from the Al(111) surface as a function of the final electron energy for the ejection angles $\theta_f = 30°, 45°, 60°$, and $90°$. Three different carrier frequencies in the range $\omega > \omega_s$ are considered: $\omega = 0.5$ a.u. [Fig. 1(a)], $\omega = 1.0$ a.u. [Fig. 1(b)], and $\omega = 2.0$ a.u. [Fig. 1(c)]. In the direction perpendicular to the surface, photoelectron spectra present a broad maximum that is associated with the above-threshold ionization (ATI) process by absorption of one photon. Keeping the number of cycles as a constant (six cycles in our case), the width of this peak increases with the frequency; that is, the peak width depends on the pulse duration, increasing as τ diminishes [47], which happens for atomic targets as well [55].

In relation to the angular dependence, the electron emission for $\omega = 0.5$ a.u. [Fig. 1(a)] is almost isotropic, being similar for

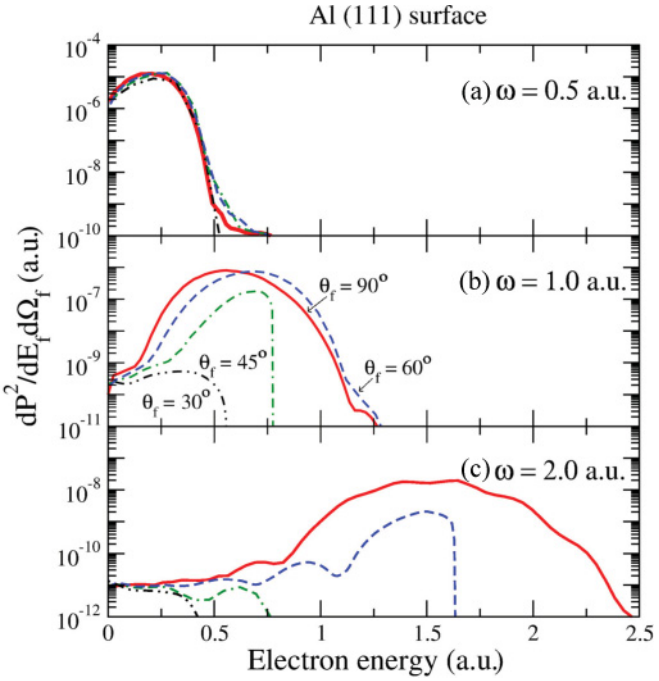

FIG. 1. (Color online) Double-differential photoelectron-emission probability from the valence band of Al(111) as a function of the electron energy for six-cycle laser pulses with carrier frequencies of (a) $\omega = 0.5$ a.u., (b) $\omega = 1.0$ a.u., and (c) $\omega = 2.0$ a.u. The peak laser electric field is $F_0 = 0.001$ a.u. The solid red line shows the BSB-V results for the ejection angle $\theta_f = 90°$, the dashed blue line shows results for $\theta_f = 60°$, the dot-dashed green line shows results for $\theta_f = 45°$, and the double-dot-dashed black line shows results for $\theta_f = 30°$.

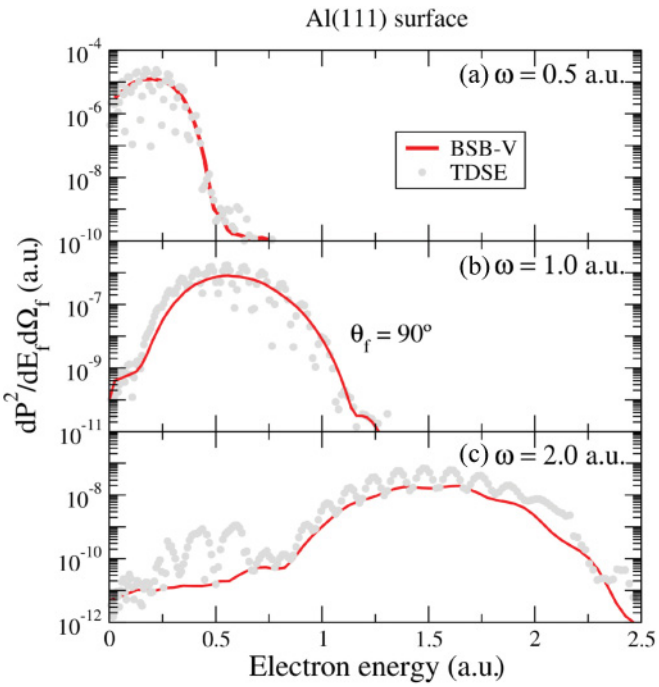

FIG. 2. (Color online) Similar to Fig. 1, but for the ejection angle $\theta_f = 90°$. The solid red line shows the BSB-V results, and gray circles present the data from the numerical TDSE calculations.

the different ejection angles. But when ω increases, electrons are mainly emitted in the direction perpendicular to the surface, which corresponds to the polarization direction of the external laser field. Furthermore, the range of final energies reached by the ejected electrons shrinks as θ_f decreases, as observed in Figs. 1(b) and 1(c). This fact is due to the momentum conservation in the direction parallel to the surface that confines the k_{fs} values within the Fermi surface, as determined by the last Heaviside function in Eq. (13). Then, the final electron energies are limited to the range $E_f \leqslant E_F/(\cos\theta_f)^2$, causing the effect that only slow electrons, with energies lower than the Fermi one, can be ejected parallel to the surface plane.

In order to determine the validity of the proposed approximation, electron distributions obtained within the BSB-V approach are compared with the numerical solution of the TDSE associated with the Hamiltonian of Eq. (1). Due to the parallel invariance of the surface and laser interactions, the TDSE problem is reduced to a one-dimensional Schrödinger equation which is solved in a numerical lattice. In such an equation the contribution of V_{ind} was again neglected because we are dealing with high carrier frequencies [47]. The time evolution from a given initial state $\phi_{n_i}(r_z)$ was performed by using an explicit "leapfrog" time propagator [56]. This method involves only one Hamiltonian matrix multiplication per time step, and it is easily implemented on massively parallel computers. Unitarity is fulfilled, providing a time step smaller than the inverse of the largest Hamiltonian eigenvalue.

After a time t_f slightly longer than the pulse duration, i.e., $t_f > \tau$, the evolved wave function is used to calculate the one-dimensional ionization amplitude a_{if} by projecting it on every particular final continuum state $\phi_{n_f}(r_z)$. In Fig. 2, BSB-V results for emission perpendicular to the surface, for which the maximum contribution to the probability at the higher frequencies is obtained, are plotted together with numerical TDSE solutions, considering the same frequencies as in Fig. 1. A good accord between BSB-V and TDSE calculations is observed throughout the whole electron energy range. Notice that this agreement holds even at high electron velocities, in the region where the emission probability has decreased several orders of magnitude, indicating the reliability of the proposed approach. On the other hand, the broad spread of TDSE values is a consequence of the defined parity of the one-dimensional wave functions that introduces spurious oscillations in the transitions amplitudes, as discussed in Ref. [57]. A solution for such a problem can be obtained by imposing the proper asymptotic conditions, and its application for our particular case is currently under development.

With the aim of investigating the effects introduced by the band structure of aluminum, in Fig. 3 BSB-V double-differential probabilities in the perpendicular direction are compared with values derived from the IJV approximation for the frequencies $\omega = 0.7$ and 2.0 a.u. The IJV approach includes a simple representation of the surface interaction that is obtained by considering that conduction electrons are bound to the surface by a finite step potential (a jellium model). Details of this calculation can be found in Ref. [34]. In the case of Al, electron spectra obtained with the BSB-V approximation are very similar to those provided by the IJV approach, displaying only a small energy shift in the position of the

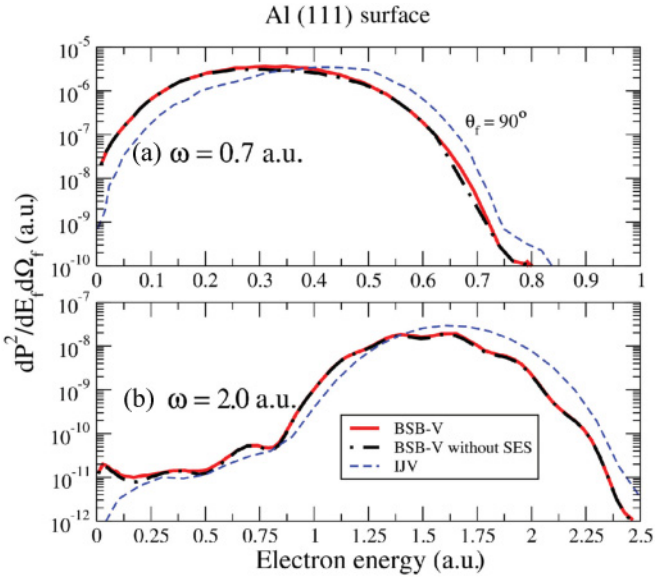

FIG. 3. (Color online) Similar to Fig. 1, but for the ejection angle $\theta_f = 90^\circ$ and two different frequencies of the pulse: (a) $\omega = 0.7$ a.u. and (b) $\omega = 2.0$ a.u. The solid red (dot-dashed black) line presents the BSB-V results including (without) SES contributions; the dashed blue line shows the IJV results.

maximum. We also analyze the importance of the presence of a partly occupied SES by evaluating its contribution to electron-emission spectra. We found that the electron distributions obtained within the BSB-V approximation including and without the SES contribution are hardly distinguishable. This fact is an additional indication of the weak influence of the realistic band structure of Al(111) in photoinduced electron-emission processes. This can be explained by a narrow bulk energy gap and a very small localization of the SES wave function on the surface [14]. Note that similar slight effects of the Al(111) band structure were also observed in ionization by proton impact [58].

B. Electron emission from Be(0001)

The Be(0001) surface is characterized by a Fermi energy $E_F = 0.506$ a.u., a work function $E_W = 0.197$ a.u., an interplanar distance of 3.387 a.u., and a surface-plasmon frequency $\omega_s = 0.47$ a.u. The BSB one-dimensional wave functions of beryllium, as given by Eq. (3), were derived by using a basis of plane waves with $N = 210$, a unit cell of width $L = 338.73$ a.u., and a distance between the crystal border and the center of the slab $d_s = 137.17$ a.u. For Be, the energy-dependent electron mean free path was obtained from Ref. [59].

BSB-V differential probabilities for electron emission from Be(0001) are shown in Fig. 4 as a function of the final electron energy for the carrier frequencies $\omega = 0.7$ and 3 a.u., which are higher than the beryllium surface-plasmon frequency. Again, electron distributions for different ejection angles ($\theta_f = 30^\circ$, 45°, 60°, and 90°) are displayed in Fig. 4. As also observed for aluminum, for the lowest frequency $d^2P/dE_f d\Omega_f$ presents a smooth variation with θ_f. The oscillatory structures of the perpendicular electron distribution corresponding to $\omega = 0.7$ a.u.

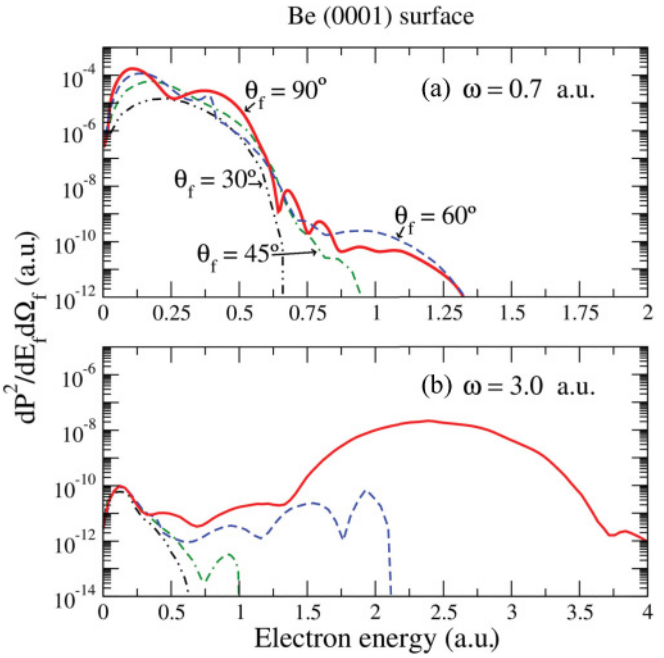

FIG. 4. (Color online) Double-differential photoelectron-emission probability from the valence band of Be(0001) as a function of the electron energy for six-cycle laser pulses with carrier frequencies of (a) $\omega = 0.7$ a.u. and (b) $\omega = 3.0$ a.u. The peak laser electric field is $F_0 = 0.001$ a.u. The solid red line presents the BSB-V results for the ejection angle $\theta_f = 90^\circ$, the dashed blue line shows the results for $\theta_f = 60^\circ$, the dot-dashed green line shows the results for $\theta_f = 45^\circ$, and the double-dot-dashed black line shows the results for $\theta_f = 30^\circ$.

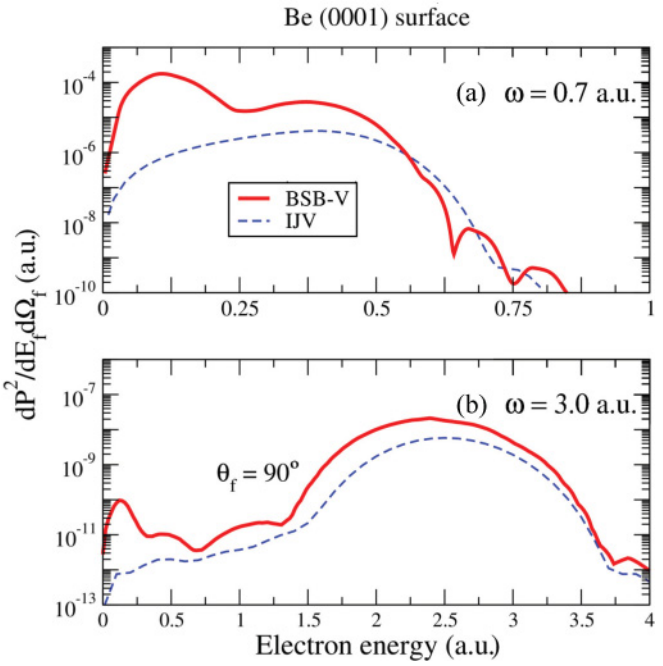

FIG. 5. (Color online) Similar to Fig. 3, but for ejection angle $\theta_f = 90^\circ$. The solid red line presents the BSB-V results, and the dashed blue line shows the IJV data.

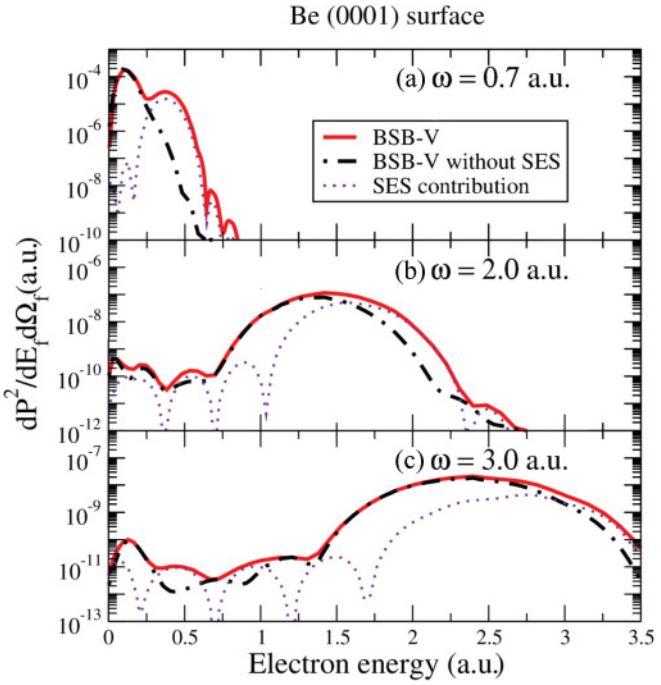

FIG. 6. (Color online) Similar to Fig. 3, but for ejection angle $\theta_f = 90^\circ$ and three different frequencies of the pulse: (a) $\omega = 0.7$ a.u., (b) $\omega = 2.0$ a.u., and (c) $\omega = 3.0$ a.u. The solid red (dot-dashed black) line presents the BSB-V results including (without) SES contributions. The dotted line shows the SES contribution only.

are gradually washed out as the ejection angle decreases. But when the frequency increases, the main contribution to the probability comes from $\theta_f = 90^\circ$, while the emission for $\theta_f \leqslant 45^\circ$ becomes almost negligible, except at the energy threshold. Note that in both cases, final electron velocities reached by the emitted electrons diminish with the emission angle, although this effect is particularly visible for high ω values [Fig. 4(b)].

To study the influence of the band structure of Be, in Fig. 5 BSB-V double-differential probabilities for $\theta_f = 90^\circ$ are compared with values derived from the IJV theory, which includes a plain representation of the surface potential. Contrary to the aluminum case, here we observe large differences between BSB-V and IJV curves, especially at low electron velocities. In this energy region the BSB-V probability displays a pronounced maximum that is not present in the IJV distribution. To understand the origin of these band-structure effects, in Fig. 6 we investigate the contribution of the partly occupied SES by plotting results derived from the BSB-V approach with and without the inclusion of the SES in the sum of Eq. (13). Three different frequencies of the laser electric field ($\omega = 0.7$, 2.0, and 3.0 a.u.) are considered in Fig. 6. We found that the maximum at the energy threshold does not relate to the SES, being produced by the corrugation of the surface potential which affects particularly slow electrons. However, the SES contribution not only originates structures at low electron energies but also modifies the spectrum for energies higher than that corresponding to the ATI maximum. This remarkable influence of the SES in the case of Be(0001) is due to the fact that this state presents a particularly high electron density near the surface border [39].

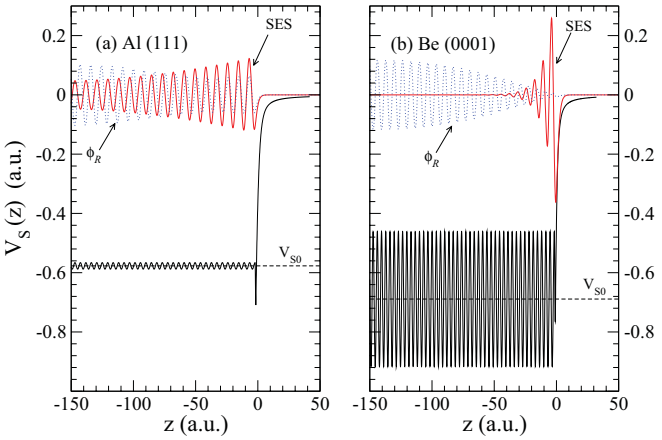

FIG. 7. (Color online) Surface potential V_S as a function of the z coordinate for (a) Al(111) and (b) Be(0001) surfaces. A comparison between the electronic wave functions (in arbitrary units) of the SES (red solid line) and a reference state ϕ_R with a close energy (blue dashed line) is shown. The crystal border is located at $z = 0$. V_{SO} denotes an average potential inside the crystal.

In order to understand the differences between Al(111) and Be(0001) photoemission spectra, we plot the corresponding surface potentials in Fig. 7. Even though the deep of the potential well, defined as $V_{S0} = E_F + E_W$, is similar for the two materials, the corrugation of the beryllium potential is more than a factor 20 larger than the one corresponding to the aluminum case, and therefore, a larger number of basis plane waves is required to reach convergence in the results. One of the consequences of this stronger corrugation of the Be potential is a stronger localization of the SES close to the surface edge. For both surfaces the electronic wave function of the SES is also displayed in Fig. 7, comparing it to the one associated with a different initially occupied state with a close energy value ϕ_R, which will be used as a reference. We observe that in the subsurface region, near the crystal border, the electronic density of the SES is higher than the one corresponding to ϕ_R and to any other bound state. However, while for Al(111) the difference between the electronic densities of the SES and ϕ_R at the surface is less than a factor of 2, for Be(0001) it rises more than one order of magnitude. Then, this highly peaked electron density of the Be SES at the surface border introduces visible effects in the double-differential electron distributions.

IV. CONCLUSIONS

We have introduced the BSB-V approximation to investigate photoinduced electron emission from the valence band of metallic surfaces. The approach includes a realistic representation of the surface interaction, incorporating information on the surface band structure of the metal. The BSB-V model was applied to evaluate double-differential electron distributions produced by grazing incidence of high-frequency laser pulses on Al(111) and Be(0001) surfaces. The reliability of the proposed method was verified by comparing BSB-V results with values derived from the numerical solution of the corresponding TDSE, finding a very good agreement. By contrasting BSB-V predictions with photoemission spectra

obtained from a simple description of the surface given by the jellium model, we conclude that band-structure effects are negligible for aluminum targets, but they become extremely important for beryllium surfaces. In particular, the BSB-V approach allowed us to analyze the contribution of partly occupied SESs separately, leading to the finding that these states produce noticeable signatures in electron-emission spectra from the Be(0001) surface, something also observed for projectile impact [43].

ACKNOWLEDGMENT

Financial support from CONICET, UBA, and ANPCyT of Argentina is acknowledged.

[1] A. L. Cavalieri *et al*., Nature (London) **449**, 1029 (2007).
[2] L. Miaja-Avila, C. Lei, M. Aeschlimann, J. L. Gland, M. M. Murnane, H. C. Kapteyn, and G. Saathoff, Phys. Rev. Lett. **97**, 113604 (2006).
[3] L. Miaja-Avila, G. Saathoff, S. Mathias, J. Yin, C. La-o-vorakiat, M. Bauer, M. Aeschlimann, M. M. Murnane, and H. C. Kapteyn, Phys. Rev. Lett. **101**, 046101 (2008).
[4] G. Saathoff, L. Miaja-Avila, M. Aeschlimann, M. M. Murnane, and H. C. Kapteyn, Phys. Rev. A **77**, 022903 (2008).
[5] L. Miaja-Avila, J. Yin, S. Backus, G. Saathoff, M. Aeschlimann, M. M. Murnane, and H. C. Kapteyn, Phys. Rev. A **79**, 030901(R) (2009).
[6] S. Mathias, M. Wiesenmayer, F. Deicke, A. Ruffing, L. Miaja-Avila, M. M. Murnane, H. C. Kapteyn, M. Bauer, and M. Aeschlimann, J. Phys. Conf. Ser. **148**, 012042 (2009).
[7] E. E. Krasovskii and M. Bonitz, Phys. Rev. Lett. **99**, 247601 (2007).
[8] C. Lemell, B. Solleder, K. Tőkési, and J. Burgdörfer, Phys. Rev. A **79**, 062901 (2009).
[9] E. E. Krasovskii, Phys. Rev. B **84**, 195106 (2011).
[10] C.-H. Zhang and U. Thumm, Phys. Rev. A **84**, 065403 (2011).
[11] I. E. Tamm, Z. Phys. **76**, 849 (1932).
[12] W. Shockley, Phys. Rev. **56**, 317 (1939).
[13] S. G. Davison and M. Stęślicka, *Basic Theory of Surface States* (Oxford University Press, Oxford, 1992).
[14] E. V. Chulkov, V. M. Silkin, and P. M. Echenique, Surf. Sci. **437**, 330 (1999).
[15] D. M. Volkov, Z. Phys. **94**, 250 (1935).
[16] E. V. Chulkov, V. M. Silkin, and P. M. Echenique, Surf. Sci. **391**, L1217 (1997).
[17] P. M. Echenique and J. B. Pendry, J. Phys. C **11**, 2065 (1978).
[18] F. Finocchi, C. M. Bertoni, and S. Ossicini, Vacuum **41**, 535 (1990).
[19] L. Jurczyszyn and M. Stęślicka, Surf. Sci. **266**, 141 (1992).
[20] N. Nekovee and J. E. Inglesfield, Europhys. Lett. **19**, 535 (1992).
[21] P. M. Echenique, R. Berndt, E. V. Chulkov, Th. Fauster, A. Goldmann, and U. Höfer, Surf. Sci. Rep. **52**, 219 (2004).
[22] E. V. Chulkov, I. Sarría, V. M. Silkin, J. M. Pitarke, and P. M. Echenique, Phys. Rev. Lett. **80**, 4947 (1998).
[23] J. Kliewer, R. Berndt, E. V. Chulkov, V. M. Silkin, P. M. Echenique, and S. Crampin, Science **288**, 1399 (2000).
[24] T. Hecht, H. Winter, A. G. Borisov, J. P. Gauyacq, and A. K. Kazansky, Phys. Rev. Lett. **84**, 2517 (2000).
[25] D. Varsano, M. A. L. Marques, and A. Rubio, Comput. Mater. Sci. **30**, 110 (2004).
[26] A. K. Kazansky and P. M. Echenique, Phys. Rev. Lett. **102**, 177401 (2009).
[27] L. Chen, J. Shen, J. J. Jia, T. Kandasamy, K. Bobrov, L. Guillemot, J. D. Fuhr, M. L. Martiarena, and V. A. Esaulov, Phys. Rev. A **84**, 052901 (2011).
[28] L. Marušic, V. Despoja, and M. Šunjić, Solid State Commun. **151**, 1363 (2011).
[29] A. Sperl, J. Kröger, and R. Berndt, J. Phys. Chem. A **115**, 6973 (2011).
[30] S. Achilli, G. P. Brivio, G. Fratesi, and M. I. Trioni, J. Phys. Chem. A **115**, 8498 (2011).
[31] J. E. Inglesfield, J. Phys. Condens. Matter **23**, 305004 (2011).
[32] M. Feng, J. Zhao, T. Huang, X. Y. Zhu, and H. Petek, Acc. Chem. Res. **44**, 360 (2011).
[33] R. Díez Muiño, D. Sánchez-Portal, V. M. Silkin, E. V. Chulkov, and P. M. Echenique, Proc. Natl. Acad. Sci. USA **108**, 971 (2011).
[34] M. N. Faraggi, M. S. Gravielle, and D. M. Mitnik, Phys. Rev. A **76**, 012903 (2007).
[35] J. C. Baggesen and L. B. Madsen, Phys. Rev. A **78**, 032903 (2008).
[36] C.-H. Zhang and U. Thumm, Phys. Rev. Lett. **102**, 123601 (2009); **103**, 239902(E) (2009).
[37] C.-H. Zhang and U. Thumm, Phys. Rev. A **80**, 032902 (2009).
[38] A. K. Kazansky and P. M. Echenique, Phys. Rev. Lett. **102**, 177401 (2009).
[39] E. V. Chulkov, V. M. Silkin, and E. N. Shirykalov, Surf. Sci. **188**, 287 (1987).
[40] M. Alducin, V. M. Silkin, J. I. Juaristi, and E. V. Chulkov, Phys. Rev. A **67**, 032903 (2003).
[41] V. M. Silkin, A. García-Lekue, J. M. Pitarke, E. V. Chulkov, E. Zaremba, and P. M. Echenique, Europhys. Lett. **66**, 260 (2004).
[42] V. M. Silkin, J. M. Pitarke, E. V. Chulkov, and P. M. Echenique, Phys. Rev. B **72**, 115435 (2005).
[43] C. D. Archubi, M. S. Gravielle, and V. M. Silkin, Phys. Rev. A **84**, 012901 (2011).
[44] E. E. Krasovskii, W. Schattke, P. Jiříček, M. Vondráček, O. V. Krasovska, V. N. Antonov, A. P. Shpak, and I. Bartoš, Phys. Rev. B **78**, 165406 (2008).
[45] E. E. Krasovskii, V. M. Silkin, V. U. Nazarov, P. M. Echenique, and E. V. Chulkov, Phys. Rev. B **82**, 125102 (2010).
[46] P. A. Macri, J. E. Miraglia, and M. S. Gravielle, J. Opt. Soc. Am. B **20**, 1801 (2003).
[47] M. N. Faraggi, I. Aldazabal, M. S. Gravielle, A. Arnau, and V. M. Silkin, J. Opt. Soc. Am. B **26**, 2331 (2009).
[48] P. Dombi, F. Krausz, and G. Farkas, J. Mod. Opt. **53**, 163 (2006).
[49] G. P. Acuña and J. E. Miraglia, Surf. Sci. **600**, 4961 (2006).
[50] V. P. Zhukov and E. V. Chulkov, J. Phys. Condens. Matter **14**, 1937 (2002).

[51] C. J. Joachain, in *Quantum Collision Theory* (North-Holland, Amsterdam, 1979), p. 378.
[52] M. I. Stockman, M. F. Kling, U. Kleineberg, and F. Krausz, Nat. Photonics **1**, 539 (2007).
[53] M. N. Faraggi, M. S. Gravielle, and V. M. Silkin, Phys. Rev. A **69**, 042901 (2004).
[54] D. R. Penn, Phys. Rev. B **35**, 482 (1987).
[55] V. D. Rodríguez, E. Cormier, and R. Gayet, Phys. Rev. A **69**, 053402 (2004).
[56] W. H. Press, S. A. Teukolsky, W. T. Vetterling, and B. P. Flannery, *Numerical Recipes* (Cambridge University Press, New York, 1992).
[57] A. E. Garriz, A. Sztrajman, and D. Mitnik, Eur. J. Phys. **31**, 785 (2010).
[58] M. N. Faraggi, M. S. Gravielle, M. Alducin, J. I. Juaristi, and V. M. Silkin, Phys. Rev. A **72**, 012901 (2005).
[59] B. Ziaja, R. A. London, and J. Hajdu, J. Appl. Phys. **99**, 033514 (2006).